Ascites analysis by a microfluidic chip allows tumor-cell profiling

Vanessa M. Peterson[a,b,1], Cesar M. Castro[a,c,1], Jaehoon Chung[a], Nathan C. Miller[a,b], Adeeti V. Ullal[a,b], Maria D. Castano[a], Richard T. Penson[c], Hakho Lee[a], Michael J. Birrer[c], and Ralph Weissleder[a,c,d,2]

[a]Center for Systems Biology, Massachusetts General Hospital, Boston, MA 02114; [d]Department of Systems Biology, Harvard Medical School, Boston, MA 02115; [c]Massachusetts General Hospital Cancer Center, Harvard Medical School, Boston, MA 02114; and [b]Massachusetts Institute of Technology, Cambridge, MA 02139

Edited* by Patricia K. Donahoe, Massachusetts General Hospital, Boston, MA, and approved October 30, 2013 (received for review August 15, 2013)

Ascites tumor cells (ATCs) represent a potentially valuable source of cells for monitoring treatment of ovarian cancer as it would obviate the need for more invasive surgical biopsies. The ability to perform longitudinal testing of ascites in a point-of-care setting could significantly impact clinical trials, drug development, and clinical care. Here, we developed a microfluidic chip platform to enrich ATCs from highly heterogeneous peritoneal fluid and then perform molecular analyses on these cells. We evaluated 85 putative ovarian cancer protein markers and found that nearly two-thirds were either nonspecific for malignant disease or had low abundance. Using four of the most promising markers, we prospectively studied 47 patients (33 ovarian cancer and 14 control). We show that a marker set (ATC_{dx}) can sensitively and specifically map ATC numbers and, through its reliable enrichment, facilitate additional treatment-response measurements related to proliferation, protein translation, or pathway inhibition.

biomarkers | molecular profiling | personalized medicine

Ovarian cancer is the deadliest of gynecologic cancers, with fewer than 50% of women surviving at 5 y following diagnosis (1). Unfortunately, this statistic has changed little over the years, and most patients are still treated with a one-size-fits-all approach (2). Such a treatment strategy does not account for the broad genomic and proteomic diversity evident within ovarian tumors. Accurate measurement of protein markers will be critical in distinguishing effective from ineffective therapies. Despite the current push for biopsy-driven clinical trials, there are no minimally invasive tests or reliable biomarker panels capable of identifying ovarian cancer treatment failures before radiographic evidence of progression. The reasons are severalfold, including heterogeneity of disease (3), variable expression levels of single biomarkers (4, 5), and markers that fail to distinguish malignant from benign disease (6, 7). However, an expanding pipeline of targeted therapies and increased appreciation for the molecular drivers within ovarian cancers have spawned a number of novel approaches for detection and treatment monitoring; these approaches include primarily blood tests for circulating tumor cells (8), tumor-derived exosomes (9), stem/progenitor cells (10), and soluble tumor markers (11, 12), as well as the use of genomic (13, 14) or proteomic information (15). Lacking, however, are practical yet highly effective point-of-care (POC) platforms that can improve currently limited clinical practices (16). We hypothesized that peritoneal fluid rather than blood might be a superior source of study material for "liquid biopsy" analyses.

Excess peritoneal fluid accumulation (ascites) in ovarian cancer is routinely drained (paracentesis) for symptomatic relief. Although often discarded, ascites could provide a source of abundant cellular material and potentially be preferable over blood samples. The precise cellular composition of ascites tends to vary across patients; the fraction of ascites tumor cells (ATCs) is generally believed to be <0.1% of harvested cells, with the remainder being host cells (37% lymphocytes, 29% mesothelial cells, and 32% macrophages) (17). The hurdle lies in reliably identifying and isolating ATCs from their highly heterogeneous environment. To help overcome these challenges, we developed a microfluidic chip platform to enrich ATCs directly from ascites and then perform molecular analyses on these cells. We evaluated 85 putative ovarian cancer protein markers and found that a reduced marker set (ATC_{dx}) can map ATC numbers. This approach is poised to expand the utility of analyzing ATCs during cytotoxic and/or molecularly targeted therapy ovarian-cancer trials.

Results

Experimental Approach. Fig. 1 summarizes the experimental approach. Surveying the literature (10, 18-26) and scientific databases (27), we tested putative diagnostic markers of ovarian cancer, mesothelial, and other host cells, as well as mechanistic markers of treatment response (19, 20, 28, 29). Initially, we tested over 100 commercially available antibodies against 85 biomarkers in 12 ovarian cancer cell lines (OV-90, OVCAR-3, SK-OV-3, ES-2, OVCA429, CaOV-3, UCI-101, UCI-107, UWB1.289, TOV-21G, TOV-112D, A2780), two mesothelial cell lines (LP9, LP3), two benign ovarian cell lines (TIOSE4, TIOSE6), and in lymphocytes and neutrophils (*SI Appendix*, Fig. S1). From these data, 31 markers were identified by flow cytometry and profiled in a training set of human ascites collected under an Institutional Review Board (IRB)-approved protocol (Fig. 2). Based on these findings, we then sought to

Significance

Serial molecular analyses of tumor cells during treatment- and biopsy-driven clinical trials are emerging norms for many cancers. Yet surgical and image-guided biopsies are expensive and invasive, explaining why alternative sources for tumor cells are being sought. In ovarian cancer (and other abdominopelvic cancers), abdominal fluid buildup (ascites) occurs frequently. We demonstrate that ascites tumor cells (ATCs) present a valuable source of tumor cells, rendering ascites another form of "liquid biopsy." We evaluated 85 ovarian cancer-related markers and developed a unique, low cost miniaturized microfluidic ATC chip for on-chip enrichment and molecular profiling using small amounts of ascites. This approach could expand the utility of ATCs within cytotoxic and/or molecularly targeted ovarian cancer therapeutic trials.

Author contributions: V.M.P., C.M.C., J.C., R.T.P., H.L., M.J.B., and R.W. designed research; V.M.P., N.C.M., and M.D.C. performed research; J.C., A.V.U., and H.L. contributed new reagents/analytic tools; V.M.P., C.M.C., H.L., and R.W. analyzed data; and V.M.P., C.M.C., M.J.B., and R.W. wrote the paper.

The authors declare no conflict of interest.

*This Direct Submission article had a prearranged editor.

[1]V.M.P. and C.M.C. contributed equally to this work.

[2]To whom correspondence should be addressed. E-mail: rweissleder@mgh.harvard.edu.

This article contains supporting information online at www.pnas.org/lookup/suppl/doi:10.1073/pnas.1315370110/-/DCSupplemental.

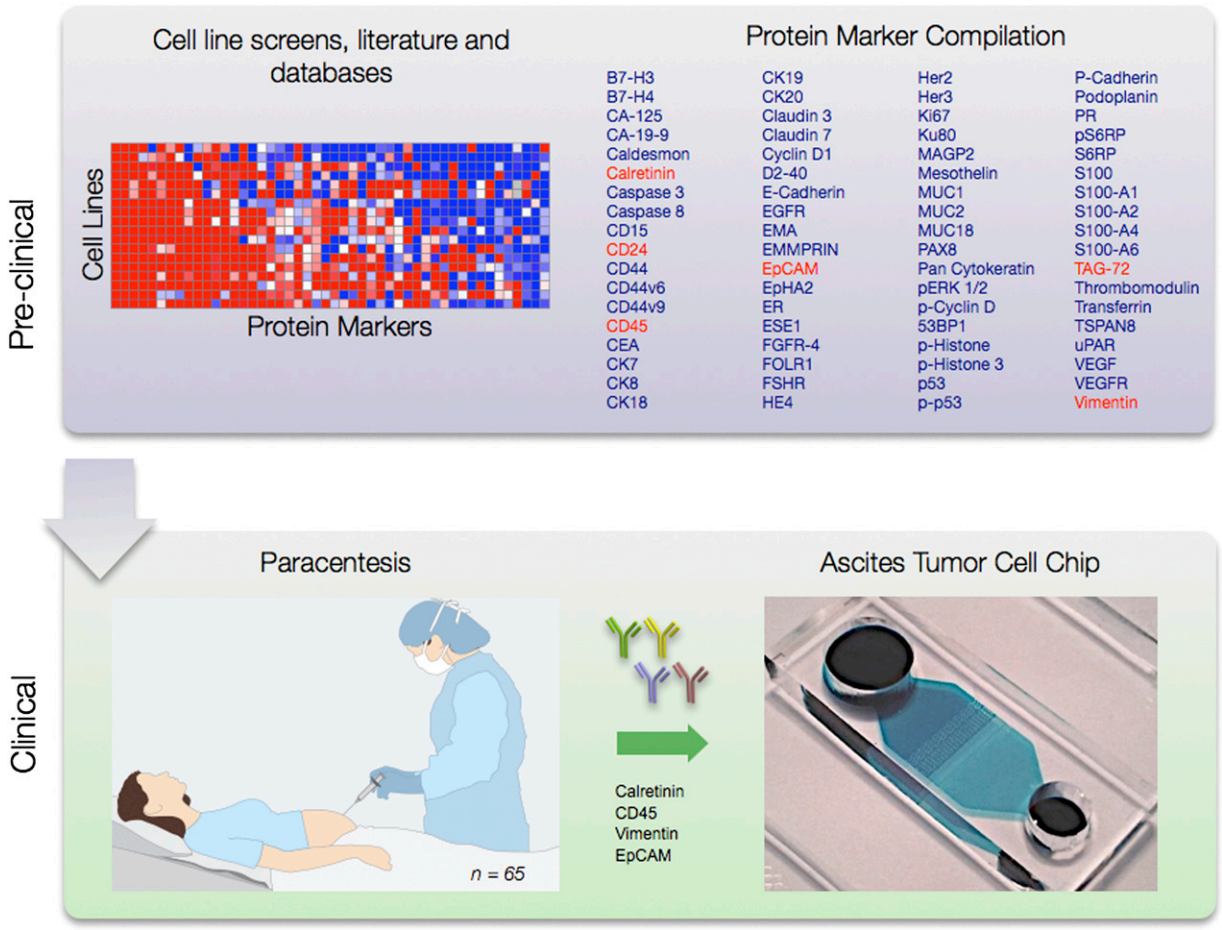

Fig. 1. Schematic approach. A total of 85 putative ovarian cancer protein markers were identified through literature, database, and other screens (*Upper Left*). Markers were tested in 12 ovarian cell lines (*SI Appendix*, Fig. S1), and a subset were examined in ascites from human patients (*Lower Left*; $n = 65$) (Figs. 2 and 3). A microfluidic chip (Fig. 4) was developed for point-of-care analysis (*Lower Right*).

establish a reliable and manageable protein-marker panel that could be adapted to microfluidic point-of-care testing. Altogether, we accrued a patient cohort involving 65 patients [$n = 46$ OvCA (Table 1), $n = 19$ benign] across training ($n = 18$ samples) and testing ($n = 47$ samples) sets (Table 2 and Fig. 3). Control samples included ascites collected from patients with end-stage liver disease or advanced heart failure without known malignancy. Based on these profiling studies, we tested aliquots of these patient samples in the ATC chip (Fig. 4) via on-chip staining (Fig. 5) or chip-based harvesting for subsequent mRNA analysis (Fig. 6). In addition, serial samples (Fig. 7) were obtained in a subset of patients during therapy ($n = 7$); these temporal samples were not included in the training or test portions of the study.

Protein Expression in a Training Set of Human Ascites Samples. The clinical training set comprised 18 patients (13 ovarian cancer, 5 nonovarian cancer). First, ascites samples were purified from cluster of differentiation 45 (CD45)-positive cells using magnetic separation. Then, multicolor flow cytometry was performed to determine marker expression levels in CD45-positive leukocytes, calretinin-positive mesothelial cells(18), and calretinin/CD45-negative cells (Fig. 2*A*). The latter were tested for multiple biomarkers (Fig. 2*B*) (see *Methods* for details). The clinical performance of each marker was determined by receiver operating characteristic (ROC) analyses adapted to flow cytometry (30, 31) (*SI Appendix*, Fig. S4). The ROC curves were used to calculate optimal cutoff values for individual markers and subsequently the sensitivity, specificity, and accuracy for each marker (30, 31).

The markers unique to cancer cells with the highest sensitivity were epithelial cell adhesion molecule (EpCAM), cluster of differentiation 24 (CD24), and tumor-associated glycoprotein 72 (TAG-72) (Table 3). Markers that were nonspecific and expressed in both cancer and mesothelial cells included vimentin, mucin 1 (MUC1), CD44, cancer antigen 125 (CA-125), folate receptor 1 (FOLR1), Wilms tumor protein (WT1), and epidermal growth factor receptor (EGFR). Markers unique to mesothelial cells included D2-40 and thrombomodulin. Noteworthy was the low sensitivity of FOLR1 (69.2%) and CA-125 (53.8%). FOLR1 has been often cited in literature as a promising therapeutic target (32, 33), and CA-125 is the most frequently used biomarker for ovarian-cancer monitoring (34). Also of note, the three ovarian-cancer patients with the lowest EpCAM expression level had the highest vimentin levels, suggestive of epithelial-to-mesenchymal transition (EMT); their median survival was 5 mo (range 1–8 mo). It is thought that, during EMT, epithelial cancer cells undergo biochemical changes resulting in a mesenchymal cell phenotype that enhances migratory capacity, invasiveness, and resistance to apoptosis (35, 36). We next identified an ascites-derived tumor signature termed ATC_{dx} referring to cells that are either $EpCAM^{+}$ and/or V3-positive ($Vimentin^{+}/Calretinin^{-}/CD45^{-}$). This ATC_{dx} panel had higher sensitivity, specificity, and accuracy than any individual marker alone and was able to correctly identify all 13 ovarian-cancer samples in the training set (Table 3).

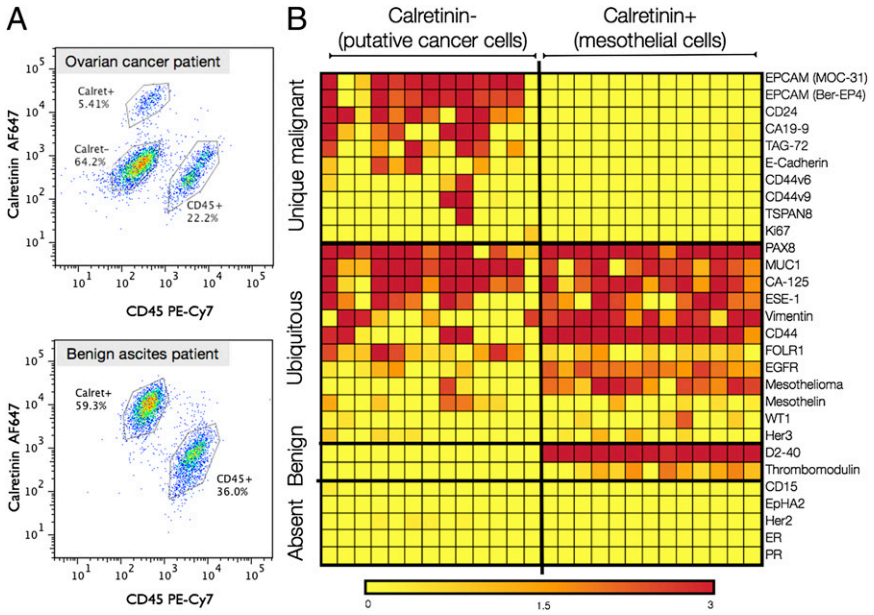

Fig. 2. Profiling of primary human samples in a training set. (*A*) Multicolor flow cytometry was used for gating of mesothelial (calretinin$^+$), leukocytes (CD45$^+$), and CD45/Calretinin$^-$ cells. (*B*) A subgroup of 31 markers identified in the cell-line screen (*SI Appendix*, Fig. S1) were subsequently tested in a training set (n = 18). The markers were placed into four different categories: unique malignant, overlapping markers (ubiquitous), benign, and absent, using cutoffs described in *Methods*. The three OvCA patients with lowest EpCAM expression levels had the highest vimentin expression levels, suggestive of epithelial-to-mesenchymal transition (EMT). This training set led to identification of the ATC_{dx} panel where malignancy is defined by either having an EpCAM$^+$ and/or V3$^+$ (Vimentin$^+$/Calretinin$^-$/CD45$^-$) signature. Heatmap values are the log ratio of the fluorescent signal over the ctrl [λ = (Sig-Ctrl)/Ctrl] where the ctrl is the secondary antibody without the primary antibody (see *Methods* for more details) (yellow, lowest; red, highest).

Prospective ATC Profiling in a Test Set of Human Ascites Samples. We next investigated the diagnostic performance of ATC_{dx} in a prospective study (Fig. 3). Using a test set of 47 patients (n = 33 OvCA, n = 14 benign), we were able to demonstrate high sensitivity and specificity. Namely, the presence or absence of ATC_{dx} correctly identified 33 ovarian-cancer patients and 14 benign ascites samples (Fig. 3*A*). In patients with sufficient cell numbers for flow analyses, the four markers with the highest sensitivity in the training set were evaluated in the test set. The cutoff values determined from ROC analyses (*SI Appendix*, Fig. S4) in the training set were applied to the test set (Fig. 3*B*). The sensitivity, specificity, and accuracy of these individual markers were then calculated (*SI Appendix*, Table S1). EpCAM had the highest sensitivity (93.9%) and accuracy (95.7%), followed by CD24 (sensitivity, 85.7%; accuracy, 89.7%). Adding V3 (Vimentin$^+$/Calretinin$^-$/CD45$^-$) to EpCAM (ATC_{dx} panel) increased sensitivity and accuracy.

Ascites Specimen Cellular Composition. The total cell and ATC count in ascites specimens was determined for each of the 65 patients (n = 46 OvCA, n = 19 Ctrl) (*SI Appendix*, Fig. S5). The mean total cell number (host cells and ATCs) for the 65 patients was 1.2×10^5 cells per mL (median, 4.1×10^4 ; range, 3×10^3 to 1.5×10^6; SEM, 2.7×10^4) and similar (P value > 0.05) in both the 46 OvCA (mean, 1.5×10^5; median, 6.8×10^4; range, 1.6×10^3 to 1.5×10^6; SEM, 3.5×10^4) and 19 control samples (mean, 6.7×10^4; median, 3.2×10^4; range, 3.1×10^3 to 5×10^5; SEM, 2.6×10^4). ATCs were identified in all 46 ovarian-cancer patients (mean, 2.7×10^4; median, 2×10^3; range, 1.5×10^1 to 6×10^5; SEM, 1.4×10^4).

ATC Enrichment and Detection Using a Point-Of-Care Microfluidic Chip. Many of the ascites samples we procured contained clumps and extracellular debris that pose a challenge for conventional microfluidic approaches (*SI Appendix*, Fig. S6). We thus developed a unique ATC chip equipped with (*i*) a miniature filter (70 μm) at the inlet to prevent downstream clogging (Fig. 4), (*ii*) negative magnetic selection of benign cells captured by

Table 1. Characteristics of ovarian-cancer patients (n = 46)

Characteristic	No.	Percentage
Ovarian-cancer patients	46	
Age		
Median	60	
Range	36–85	
Stage		
IC	1	2
IIIC	27	59
IV	18	39
Surgical debulking		
Optimal	25	55
Suboptimal	6	13
Interval	14	30
None	1	2
Survival (avg mo from collection)		
Alive	14 (26)	30
Deceased	32 (9)	70
Chemotherapy		
Active	21	45
Not yet initiated	25	55
Platinum response		
Sensitive	18	39
Resistant	18	39
Refractory	4	9
Not applicable	6	13
Disease course		
Response	19	41
Stable	1	2
Progression	24	52.5
Mixed	2	4.5

Table 2. Sample numbers of different data sets

Dataset	Definition	Malignant (*n*)	Benign (*n*)	Total (*n*)
Profiling	Profiling of cell lines; no primary patient samples	12	6	18
Training	Validation of markers identified in cell screens	13	5	18
Test	Prospective analysis in patient cohort	33	14	47
Complete	All above patient samples combined	46	19	65
Serial Tx	Patients with repeat samples	7	NA	7

a magnet located under the device inlet, and (*iii*) multiple, serially smaller microwells (40–15 μm) in which purified and enriched cells are captured (*SI Appendix*, Fig. S7). The multistep, on-chip purification approach yielded an approximate 1,000-fold ATC enrichment (*SI Appendix*, Fig. S8). Perhaps more important, the microwell-captured cells facilitated visualization of the cell populations and simplified multicolor image analysis.

The ATC chip was designed to be optically transparent so that cells captured in microwells, can be stained on-chip and visualized with a charge-coupled device (CCD). Fig. 5 illustrates a representative example of ATC_{dx}-based staining of ATCs (red), and CD45/Calretinin staining of mesothelial and host cell staining (green). Compared with conventional flow-cytometry needs (~10,000 cells), the ATC chip affords reduced sample-size requirements due to its single cell detection capabilities. For example, an ovarian-cancer patient harboring 15 ATCs per mL would require >500 mL of ascites processing for flow cytometry compared with only 0.1 mL for on-chip processing. Moreover, this microfluidic chip can be fabricated using soft lithographic techniques (37, 38) with inexpensive materials such as PDMS, providing a practical, affordable (<$1.00 per chip), and scalable alternative to flow cytometry. We also demonstrated that chip-enriched cells (Fig. 6*A*) can be further analyzed such as for mRNA expression levels. Measurements of mRNA on cells from the ATC chip showed excellent correlation to bulk measurements ($R^2 = 0.995$) (Fig. 6*B*). Ascites samples from five ovarian-cancer patients were enriched with ATC chip and subsequently profiled for gene-expression levels relative to benign cell lines (Fig. 6*C*). EpCAM and CD24 had the highest expression levels concurrent with our earlier findings in the training and test sets (Table 3 and *SI Appendix*, Table S1).

Serial Testing to Measure Treatment Response in Individual Patients. A major application of a point-of-care approach would be to leverage the use of readily accessible (but otherwise discarded) ascites as a source of ATCs for treatment monitoring. Fig. 7 exemplifies this potential using ascites collected and profiled from a single patient over a 14 wk treatment period. The patient was initially treated with cytotoxic agents (Carboplatin and Paclitaxel; weeks 2 and 5) but was transitioned to antiangiogenic

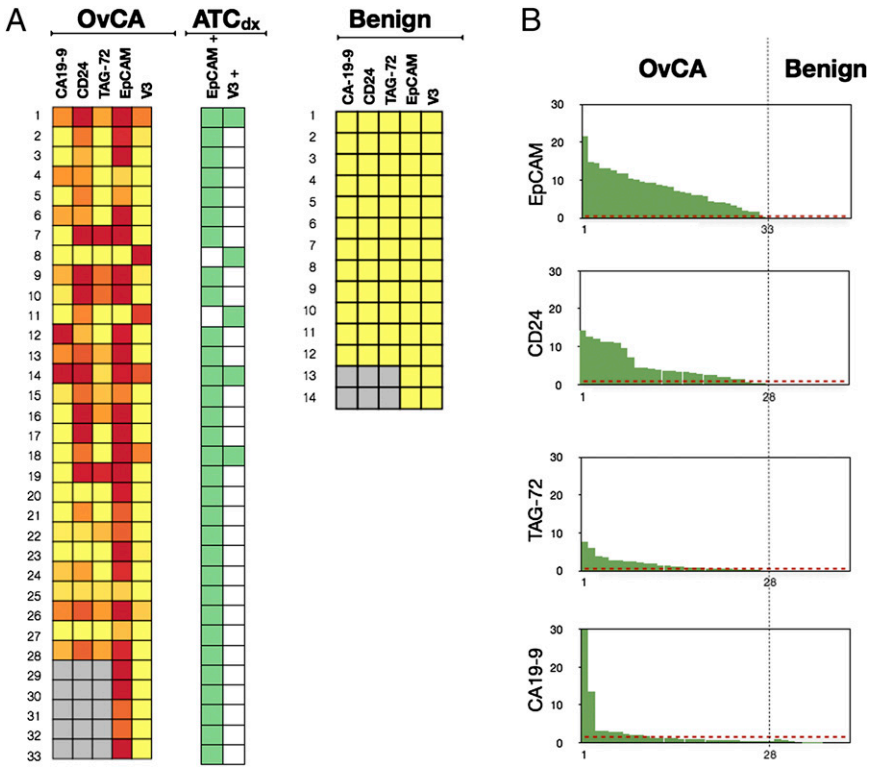

Fig. 3. Prospective testing of ATC marker panels in 47 patients. (*A*) Ascites samples were tested for the presence of six individual markers in 33 ovarian-cancer patients (*Left*) and 14 controls (right). EpCAM alone was positive in 31 samples. By using the V3 marker set (Vimentin$^+$/Calretinin$^-$/CD45$^-$) and EpCAM together (ATC_{dx}), all 33 samples were correctly identified (green heat map). ATCs were identified in malignant samples, but not in benign samples. Gray squares represent data not measured due to insufficient number of cells for flow cytometry. Color scale is same as Fig. 2*B*. (*B*) Waterfall plots of the individual markers profiled in the test set. Dotted red lines represent the optimal threshold values determined from ROC analyses performed on the training set (*SI Appendix*, Fig. S4).

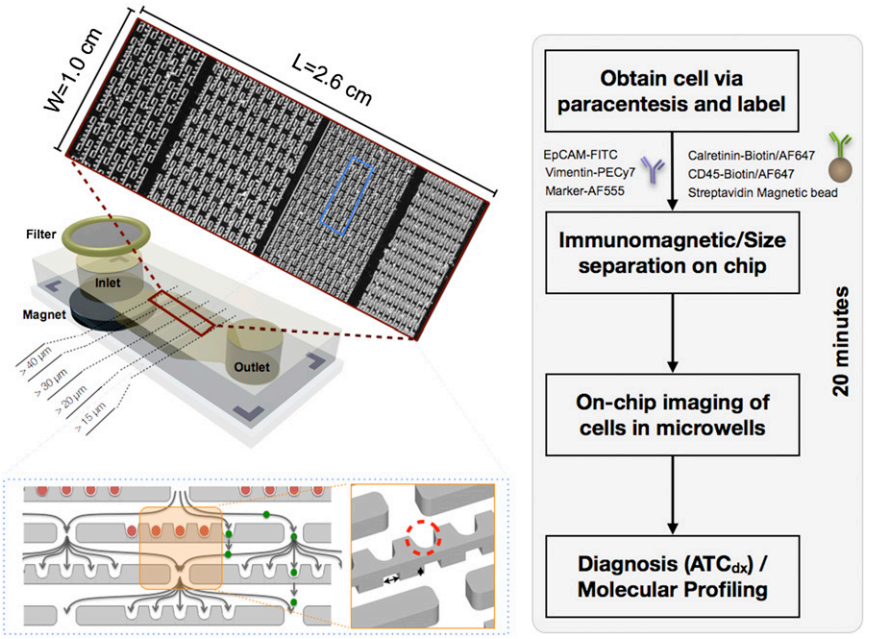

Fig. 4. Schematic of on-chip purification and labeling. First, ascites fluid is collected from the patient that contains malignant cells among an inflammatory milieu of host cells. Ascites cells are added to the chip followed by an antibody mixture (EpCAM-FITC, Vimentin-PE/Cy7 Calretinin-Biotin/AF647, CD45-Biotin/AF647, Marker-AF555). Streptavidin-coated magnetic particles then bind to the benign mesothelial cells (Calret$^+$) and leukocytes (CD45$^+$). A magnet under the inlet captures the benign cells whereas the malignant cells pass freely through the microchip. The four different size microwells (15, 20, 30, and 40 μm) allow for capture of the malignant cells while allowing for the typically smaller leukocytes to pass through the device. The ATC_{dx} signature (EpCAM$^+$ and/or Vimentin$^+$/Calretinin$^-$/CD45$^-$) can then be imaged to determine number of ATCs.

therapy (Bevazucimab/Avastin; week 7) due to disease progression. ATC numbers were initially observed to decrease steadily during treatment response, only to increase when disease progression occurred. Avastin attenuated the increase in ATC burden concurrent with the patient's improved clinical symptoms.

ATC analysis could also be used for early detection of treatment response through the profiling of protein markers related to biological processes such as proliferation [Ki67, phospho histone H3 (pH3), pCyclin D], mRNA translation [phospho 4E-binding protein 1 (p4E-BP1)], and/or pathway inhibition [phospho S6 ribosomal protein (pS6RP), phospho extra-signal-regulated kinase (pERK)]. As expected, the proliferation markers Ki67, pH3, and pCyclinD had a decreasing trend mirroring ATC counts. After each Carboplatin/Taxol administration, the levels of the growth pathway markers p4E-BP1, pERK, and pS6RP were reduced and stable, but, upon switching to single agent Avastin, the levels of these markers increased. In this clinical example, the data suggest that resuming cytotoxic therapy (which had maintained pathway inhibition) alongside Avastin treatment might have slowed this patient's rapid clinical decline. Indeed, recent late-phase clinical-trial data have reported progression-free survival advantages when cytotoxic and antiangiogenic strategies are combined in ovarian cancer (39).

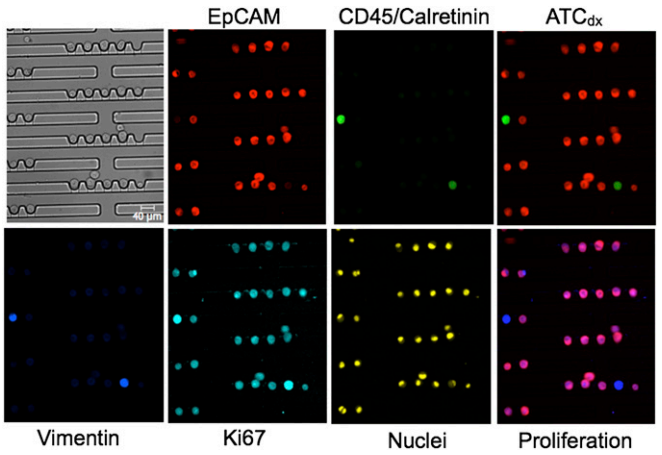

Fig. 5. On-chip ATC_{dx} and profiling. Multiple stains performed on-chip allow diagnosis of cancer cells (red) and evaluation of specific biomarkers (Ki67 in this example). The *Lower Right* image is the merge of the proliferation marker Ki67 with the ATC markers EpCAM and Vimentin. Red, EpCAM; green, CD45/Calretinin (benign host cells); blue, Vimentin; cyan, Ki67; yellow, nuclei. Note alignment of cells of chip and simple image analysis.

Using an expanded set of mechanistic markers (*SI Appendix*, Fig. S9), we also compared the profiles of treatment responders with nonresponders (based on tumor burden, as determined by imaging or clinical course) (Table 1). The panels indicate that the two groups could be distinguished based on ATC molecular profiles. Moreover, these profiles could be potentially useful for providing additional biological insight into the drivers of treatment response or disease progression. For example, unlike in treatment responders, levels of pS6RP and p4E-BP1 (readouts of the phosphatidylinositol 3/PI3-kinase pathway) remained elevated after therapy in the nonresponders. These trends are consistent with previous findings that have associated activated PI3-kinase signaling with chemoresistance in advanced ovarian cancer (40).

Discussion

In the current study, we developed and tested a bedside-compatible "ATC chip" simplifying enrichment and molecular analysis of shed cancer cells in peritoneal fluid. Unlike in blood, cells harvested from the peritoneum often form clumps and can contain extracellular debris that challenges conventional microfluidic devices. We circumvented this challenge by microfiltration, negative magnetic separation, and positioning of individual cells in

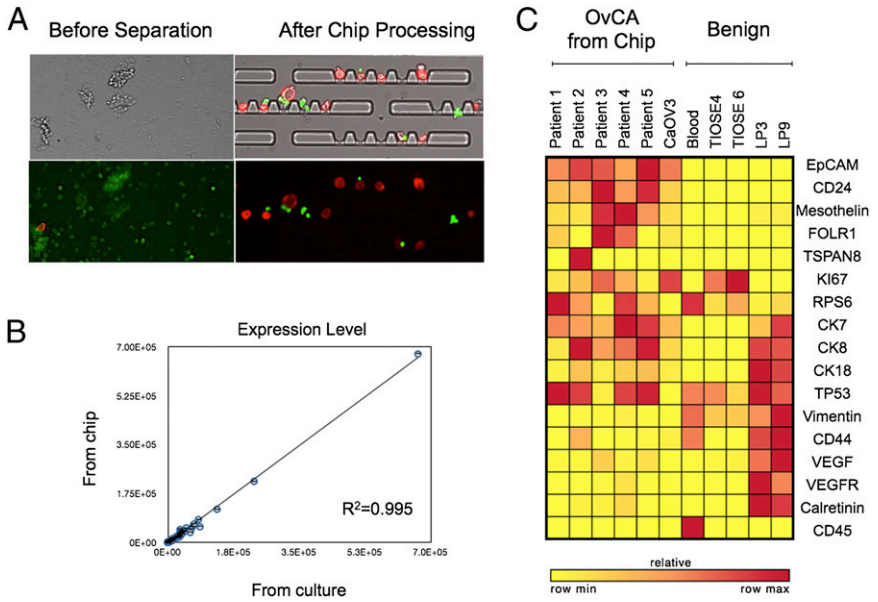

Fig. 6. On-chip Processing. (*A*) Processing ascites samples on-chip enables purification of ATCs (red) from benign cells (green) for easy detection of ATCs. (*B*) OvCA cells can be removed from chip after enrichment for downstream molecular profiling. Gene counts from CaOV3 cells isolated from chip had excellent correlation to unprocessed CaOV3 cells (R^2 = 0.995). Measurements from chip were done in triplicate, and error bars represent the SD. (*C*) Demonstration of on-chip processing in clinical samples. Ascites samples were enriched for ATCs on-chip, and then ATCs were removed and mRNA gene expression levels were measured. The heatmap shows relative expression levels for each marker (yellow, lowest; red, highest).

chip microwells that allow convenient analysis. We show that both protein analysis through on-chip staining and mRNA analysis using chip-harvested cells are feasible and result in clinically valuable information. Moreover, the device leverages the advantages of microfabrication and microfluidics to facilitate point-of-care and ascites testing, respectively. The ATC chip's low cost (<$1 per unit), ease-of-scalability (plastics), and simplicity of use could promote widespread testing and, if clinically validated,

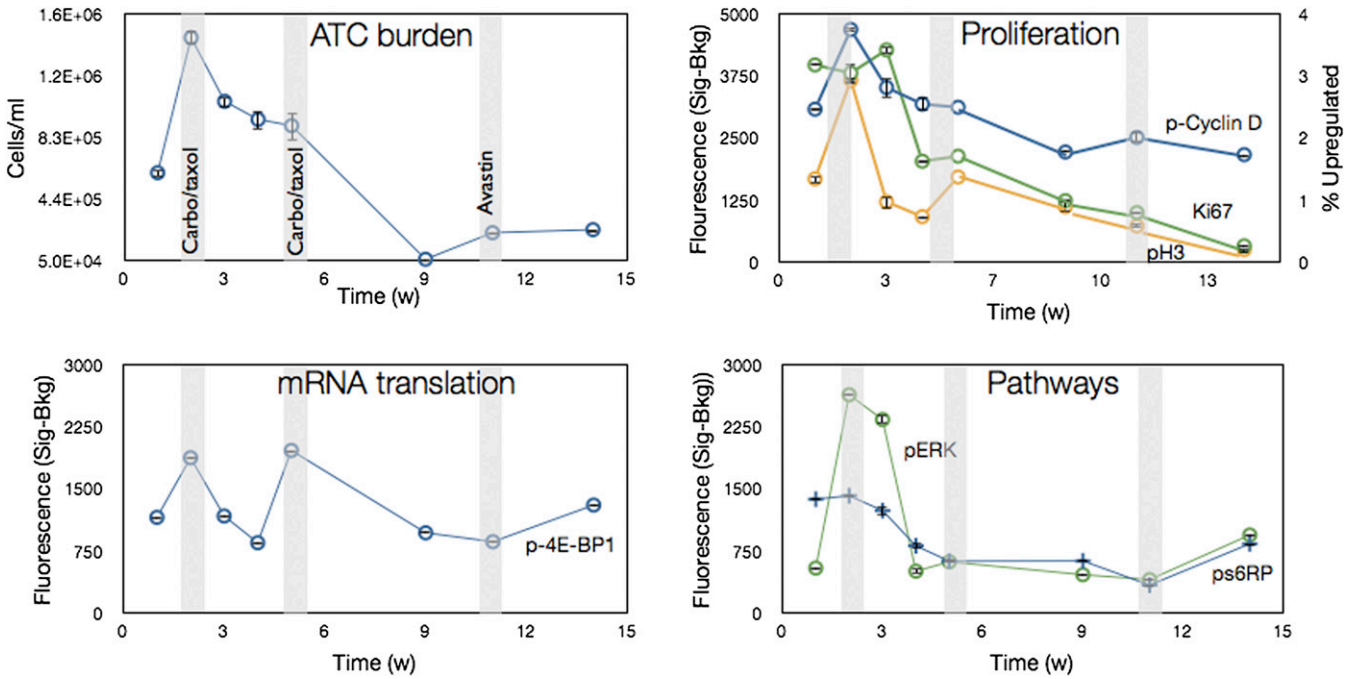

Fig. 7. Serial analysis of ATCs. ATCs were obtained serially from a single patient over a 14-wk treatment cycle. Carboplatin and Paclitaxel (Taxol) were given in weeks 2 and 5, and Bevazucimab (Avastin) was given in week 11. The number of ATCs was measured over the course of treatment (ATC burden) using ATC_{dx}. Additionally, protein markers related to biological processes such as proliferation (Ki67, pH3, pCyclinD), mRNA translation (p4E-BP1), and pathway inhibition (pS6RP, pERK) were also measured. The broader analyses demonstrate molecular profiling of ascites can be used as a tool to monitor treatment response over the course of therapy. All samples were stained with calretinin and CD45 antibodies to exclude mesothelial cells and and leukocytes, respectively. Data are expressed as the average of the mean fluorescent intensity subtracted from background ± SEM. pH3 data are plotted as % of cells up-regulated.

Table 3. Sensitivity, specificity, and accuracy of different protein markers in the training set

Markers	Sensitivity, %	Specificity, %	Accuracy, %
EpCAM	92.3	100.0	96.9
CA19-9	46.2	100.0	78.1
CD24	92.3	94.7	93.8
TAG-72	76.9	100.0	90.6
FOLR1	69.2	78.9	75.0
CA-125	53.8	94.7	78.1
V3 panel (Vim+/Calret-/CD45-)	23.1	100.0	68.8
ATC_{dx} (EpCAM+ and/or V3+)	100.0	100.0	100.0

ready adoption by tertiary academic medical centers or community hospitals.

To help address uncertainties in the biomarker literature, we ourselves screened over 100 commercially available antibodies to investigate 85 putative targets of ovarian-cancer cells in peritoneal fluid. Although we were able to identify a relatively simple marker set for these cells, we found some unexpected results. For example, we found low levels of certain markers that have been gaining traction as drug targets (EphA2) (26, 41-43), or that have been touted as specific for (CA-125, FOLR1) (32), or overabundant in (mesothelin) (44), ovarian cancer. We found relatively high expression levels of EpCAM, CD24, and TAG-72 in cancer patients, consistent with previous reports (10, 21, 45-49). In contrast, levels of calretinin (50, 51) and D2-40 (51) were high in mesothelial cells but not in ovarian-cancer cells and thus served as convenient distinction markers. MUC1, EGFR, PAX8, and ESE-1 displayed mixed expression levels that were nonspecific.

Despite the number of markers tested, there were some limitations. Firstly, the list of proteins, although lengthy, was certainly not exhaustive. Secondly, only commercially available antibodies were tested because our intention was to leverage screening findings for eventual and feasible widespread testing using the point-of-care device. It is possible that certain research antibodies might have resulted in higher and more specific binding, but this conjecture would need to be tested in additional datasets beyond the scope of the current study. Thirdly, despite screening a number of available antibodies (*SI Appendix*, Table S2), we were unable to identify reliable antibodies for FSHR (follicle-stimulating hormone receptor), a target implicated in ovarian cancer (52-55) (*SI Appendix*, Fig. S1). We thus abandoned current efforts due to low specificity, but FSHR nevertheless remains a marker of interest that requires further exploration.

In summary, we show that ascites analysis via microfluidic chips could become a convenient strategy for serially measuring ATC numbers and analyzing their molecular profile. Leveraging this additional tumor source could help expand the clinical strategies needed for paradigm shifts in patient-oriented research (56).

Methods

Patient Population and Analyses. The study was approved by the Dana Farber/Harvard Cancer Center Institutional Review Board (IRB), and informed consent was obtained from all subjects. Sixty-five subjects with accumulation of ascitic fluid, and requiring drainage, were enrolled in this study. Forty-six subjects carried a known diagnosis of ovarian cancer (Table 1) wheras 19 subjects were included as controls (e.g., their ascites fluid was as a result of another disease such as cirrhosis or liver failure). Ascites fluid samples were collected from patients per routine in the Massachusetts General Hospital (MGH) Abdominal Imaging and Intervention suites. Two clinicians (C.M.C and R.W.), blinded to the results, reviewed all of the documented clinical, imaging, and pathology data obtained from each cancer patient. Table 2 summarizes the different cohorts included in the training set (n = 18), validation set (n = 47), and serial analyses sets (n = 7).

Cell Culture. The cell lines SK-OV-3, OVCAR-3, A2780, CaOV-3, OV-90, ES-2, TOV-112D, TOV-21G, and UWB1.289 were purchased from American Type Culture Collection and grown in media following their suggested protocol. UCI-101 and UCI-107 cell lines were kindly provided by G. Scott Rose (University of California, Irvine, CA) and OVCA429 was kindly provided by David Spriggs (Memorial Sloan Kettering, New York). UCI 101, UCI 107, and OVCA429 were grown in RPMI (Cellgro) with 10% (vol/vol) FBS, 1% L-glutamine, and 1% penicillin/streptomycin. Mesothelial cells, LP3 and LP9, were purchased from the Corriell Institute for Medical Research and grown according to protocol. NOSE cell lines were derived from ovarian surface epithelium (OSE) brushings cultured in 1:1 Media 199:MCDB 105 (Sigma-Aldrich) with gentamicin (25 μg/mL) and 15% heat-inactivated serum. TIOSE4 and TIOSE6 cell lines were obtained from transfection of hTERT into NOSE cells maintained in 1:1 Media 199:MCDB 105 with gentamicin (25 μg/mL), 15% heat-inactivated serum, and G418 (500 μg/mL) (57). Cells were cultured at low passage number under standard conditions at 37 °C in a humidified incubator containing 95% room air and 5% CO_2 atmosphere. When the cells reached ~90% confluence, they were trypsinized to remove the cells from the culture flask. Medium was then added, the cells were spun down (300 × g for 5 min), and the supernatant was removed. The cells were then fixed following the same protocol as used for clinical samples; namely, Lysis/Fix buffer (BD Phosflow Lyse/Fix Buffer) was added to the cells for 10 min at 37 °C, before being washed twice with 5 mL of SB+ (PBS with 2% BSA). The cells were aliquoted into tubes (~1×10^6 cells per mL) and stored at −20 °C until labeling. The cells were then labeled following the same protocol used for clinical samples, with the exception that calretinin and CD45 antibodies were not added to each sample.

Bulk Ascites Processing for More Extensive Profiling. Clinically obtained ascites samples were transferred into 2–4 separate 225-mL conical bottom tubes (BD Falcon) and centrifuged at 300 × g for 5 min (Eppendorf Centrifuge 5810R). The supernatant was then removed, leaving the cell pellet undisturbed. The remaining ascites fluid was added to the tubes, and the centrifugation and aspiration step was repeated until all of the fluid was processed. The cell pellet in each tube was then resuspended in SB+ and transferred to a smaller 50-mL tube. The cells were spun down at 300 × g for 5 min, and the supernatant was aspirated. After vortexing, 40 mL of prewarmed Lysis/Fix buffer (BD Biosciences) was added, and the sample was incubated on a shaker at 37 °C for 10 min. If there were visual clumps present before the fixation step, collagenase (Sigma Aldrich) was added at 0.2 mg/mL in PBS, and the sample was incubated on a shaker for 30–60 min at 37 °C. The cells were then washed with SB+ before proceeding to the lysis/fix step (described above). After the lysis/fix step, the cells were centrifuged at 400 × g for 3 min, and the supernatant was removed. Then two washes with 5 mL of SB+ (PBS with 2% BSA) were conducted. The supernatant was removed after the final wash, and the cells were resuspended in 1 mL of SB+.

CD45 negative selection. Cells were counted with the Countess Cell Counter (Life Technologies) and adjusted to a concentration of ~2×10^7 cells per mL. CD45 antibody (Biolegend; H130) was added (0.5 μL per 10^6 cells) and incubated for 1 h, before washing twice with 5 mL of SB+. The supernatant was removed, and Anti-Mouse IgG1 magnetic beads (80 μL per 10^7 cells; Miltenyi Biotec) were added along with SB+ (20 μL per 10^7 cells). The reaction was incubated for 15 min at 4 °C and was followed by two washes (2 mL per 10^7 cells) with SB+. The remaining sample was then resuspended in 1 mL of SB+. Magnetic separation columns (LS; Miltenyi Biotec) and the QuadroMACS separator were used for negative selection following suggested protocols. Preseparation filters (Miltenyi Biotec) were used to remove any clumps or debris from the clinical specimens to prevent obstruction of the column. The maximum number of cells used in each column was 1×10^8. The sample was added to the column and was washed three times with 3 mL of SB+. The $CD45^-$ cells that passed through the column were subsequently collected into a 15-mL tube and centrifuged (400 × g, 3 min); the supernatant was removed, and the cells were resuspended in SB+. Cells were then counted and aliquoted into tubes at approximately ~1×10^6 cells per mL, before being stored at −20 °C until labeling.

Labeling. CD45-depleted cells stored in the −20 °C freezer were thawed. The cells were then centrifuged at 400 × g for 3 min, and the supernatant was removed. Perm buffer (PW+: BD perm/wash with 2% BSA) was added, and the cells were aliquoted into cluster tubes (Costar). The appropriate antibody mixture of calretinin and CD45 was added (*SI Appendix*, Table S2) (calretinin, Mouse Dako DAK-Calret 1 or Rabbit Invitrogen DC8; CD45, Rat Abcam YTH24.5 or Mouse Biolegend H130). The specific antibody for the biomarker of interest was then added (*SI Appendix*, Table S2). The final reaction volume was 150 μL. This primary reaction was vortexed and incubated for 1 h before 0.5 mL of PW+ was added to each sample and the cells spun down at 400 × g for 3 min. The supernatant was removed, and the

cells were vortexed and washed with 0.5 mL of PW+. After centrifugation (400 × *g*, 3 min), the supernatant was aspirated, and the appropriate secondary antibodies were added (*SI Appendix*, Table S3) [Anti-Mouse FITC Abcam (1:300); Anti-Rabbit APC Abcam (1:300); Anti-Rat PeCY7 Biolegend (1:300)]. The final reaction volume was 150 μL. The samples were vortexed and incubated on ice for 1 h. Cells were then washed twice with 0.5 mL of PW+. Samples analyzed by flow cytometry the same day were kept on ice under aluminum foil. Samples run the following day were lightly fixed [BD Phosflow Fix Buffer (1:2)] for 10 min at 37 °C and then washed with SB+. After washing, DAPI was added to the samples at a ratio of 1:500 (Fxcycle stain; Invitrogen) 30 min before analysis by flow cytometry. Antibody information (such as clone and company) for all markers is included in *SI Appendix*, Tables S2 and S3.

Flow cytometry. Fluorescently labeled samples were analyzed using an LSRII flow cytometer (Becton Dickinson). FlowJo software was used to gate on: singlets using DAPI staining, then Calretinin$^+$, CD45$^+$, and CD45$^-$/Calretinin$^-$ cell populations in the clinical samples. The mean fluorescent intensity (MFI) for each marker of interest was then determined for each of these three populations. The background was determined by staining with the secondary antibody only (no primary). The signal-over-background was then calculated [λ = (Signal-Background)/Background] and plotted in the heat maps using GENE-E software (Broad Institute). For Fig. 2 and *SI Appendix*, Fig. S1, each marker was placed into four categories on the following criteria: (*i*) "Unique Malignant" (if an ovarian-cancer sample had $\lambda > 1.5$ and all benign samples had $\lambda < 1.5$); (*ii*) "Ubiquitous" (if an ovarian-cancer sample and a benign sample had $\lambda > 1.5$); (*iii*) "Benign" (if both an ovarian-cancer sample and benign sample had $\lambda < 1.5$); and (*iv*) "Absent" (if both ovarian-cancer and benign samples had $\lambda \leq 1.5$). Figs. 2 and 3 were plotted on a log scale, and gray signifies data that was not determined. A log scale was used because this resulted in a more symmetric distribution. Histograms of a select set of markers from the cell line screening and training set are shown in *SI Appendix*, Figs. S2 and S3.

Statistical analysis. Receiver operating characteristic (ROC) curves were constructed for cancer markers relative to benign mesothelial cells in the training set (*SI Appendix*, Fig. S4). For each marker sensitivity versus (1 − specificity) was plotted, and the values of area under the curve (AUC) were computed using the trapezoidal rule. The empirical ROC curves were smoothed by applying the binormal fitting model. An AUC of 0.5 was used to indicate that the test shows no difference between the two groups whereas an AUC of 1.0 was used to indicate that the test gives a perfect separation between the groups. We defined the optimal cutoff value for identifying malignant status as the point on the ROC curve with the minimal distance between the 0% false-negative and the 100% true-positive rate. Statistical analysis was performed using the R-package (version 3.0.1). Using standard formulas, we calculated sensitivity, specificity, and accuracy.

ATC Device Fabrication. The microfluidic device was designed to contain ∼5,000 capture sites ranging in size from 15 to 40 μm (*SI Appendix*, Fig. S7*A*) in a 2.6 × 1.0 cm area. The capture sites on the device have bowl-like structures with an underpass gap that allows smaller cells to pass through. As shown in *SI Appendix*, Fig. S7*B*, path A through the capture structure has a considerably shorter length, therefore smaller flow resistance, than path B through the channel structure. Due to the flow-resistance difference, most of the fluid flows through path A rather than path B. Cells larger than the capture structures will be trapped, and smaller cells will pass through. The flow rate of the device was ∼10 mL/h and allowed ∼1,000-fold ATC enrichment (58, 59). Microfluidic single cell capture arrays were fabricated in polydimethylsiloxane (PDMS; Dow Corning) using soft lithography(37, 38). Three layers of epoxy-based photoresist were patterned on 4-in silicon wafers as a mold using conventional photolithography. The first SU8 2015 (Microchem) layer defined a 15-μm gap height in the capture sites for the 15- and 20-μm cells. Before developing unexposed SU8, the second SU8 2015 layer was coated and aligned to the channel structure for the 15- and 20-μm cell capture sites. This layer also defined the gap height (30 μm) for the 30- and 40-μm cell capture sites. Finally, another 30-μm-thick SU8 2025 was applied for the 30- and 40-μm cell capture structures. All unexposed SU8 photoresist layers were then developed in the SU8 Developer (Microchem). The mold with the channel and cell-capture patterns was silanized with a vapor of trimethylchlorosilane (TMCS; Sigma) and was cast with 3-mm-thick PDMS prepolymer. After curing, the PDMS layer was peeled off, and an inlet and an outlet were punched out. The prepared PDMS chip was then bonded (not permanently) to a glass slide. The chip thus remained detachable for easy recovery of cells after purification and imaging to enable further molecular profiling of cells.

Processing Cells Through the ATC Chip. For on-chip enrichment and staining of ATCs, ∼100 μl of ascites fluid was added to the inlet of the chip. Then, an antibody mixture of the following antibody conjugates was added: Calretinin-Biotin (Invitrogen; Rabbit), CD45-Biotin (Abcam; Mouse), CD45-Alexa Fluor 647 (Biolegend; Mouse), EpCAM-FITC (Dako; Mouse), Vimentin (R&D; Rat), and Ki67-Alexa Fluor 555 (BD Pharmingen). This mixture was incubated for 15 min. Then, streptavidin-coated magnetic particles (R&D), Anti-Rabbit Alexa Fluor 647 (Cell Signaling), and Anti-Rat PE/Cy7 (Biolegend) were added, followed by a 15-min incubation (Fig. 4). In the first enrichment step, a magnet was placed under the inlet preventing the benign CD45 and Calretinin magnetically labeled cells from passing through the chip. The non-magnetically labeled ATCs entered into the microchip when negative pressure was applied to the outlet of the device (via rubber bulb). The second enrichment step was based on size: (*i*) the typically larger ATC cells were captured on the chip's capture sites (decreasing in size from 15 to 40 μm) and (*ii*) the smaller leukocytes (∼<15 μm) (60) passed through the capture sites. This dual enrichment approach using both immunomagnetic labeling and size separation (58, 59) improved chip performance and enabled an approximate 1,000-fold enrichment to be achieved (*SI Appendix*, Fig. S8). Three washes of 100 μl of SB+ with DAPI (4′,6-diamidino-2-phenylindole; Invitrogen; 1:500) were then passed through the microchip. Captured ATCs were imaged using the DeltaVision screening system (Applied Precision Instruments) and analyzed using ImageJ software (version 10.2). Enriched cells could then be removed from the detachable chip for further molecular profiling. Measurements for mRNA expression levels were done using nCounter gene expression assay (NanoString) on cell lysate (61, 62). Data were analyzed using nsolver analysis software 1.1 (NanoString), and the heatmap (Fig. 6*C*) was plotted using GENE-E (Broad Institute).

ACKNOWLEDGMENTS. We thank M. Pectasides and S. McDermott for sample collection; C. Krasner, L. Sullivan, and S. McIlvenna for patient referral; V. Vathipadiekal and P. Waterman for help growing cell lines; H. Saya (IAMR, Keio University) for CD44v9 antibody, L. Lizotte (REMS media services) for microchip pictures, A. Zaltsman for imaging, and Y. Fisher-Jeffes for review of the manuscript. This work was funded in part by Grants P50CA086355, R01EB004626, R01EB010011, P01-CA139980, U54-CA151884, K12CA087723-11A1, and DOD W81XWH-11-1-0706. V.M.P. was supported in part by a Merck Educational Assistance Fellowship.

1. Siegel R, Naishadham D, Jemal A (2013) Cancer statistics, 2013. *CA Cancer J Clin* 63(1):11–30.
2. Na YJ, et al. (2009) Ovarian cancer: Markers of response. *Int J Gynecol Cancer* 19(Suppl 2):S21–S29.
3. Bast RCJ, Jr., Hennessy B, Mills GB (2009) The biology of ovarian cancer: New opportunities for translation. *Nat Rev Cancer* 9(6):415–428.
4. Lutz AM, et al. (2011) Early diagnosis of ovarian carcinoma: Is a solution in sight? *Radiology* 259(2):329–345.
5. Zhang B, Cai FF, Zhong XY (2011) An overview of biomarkers for the ovarian cancer diagnosis. *Eur J Obstet Gynecol Reprod Biol* 158(2):119–123.
6. Nolen BM, Lokshin AE (2012) Protein biomarkers of ovarian cancer: The forest and the trees. *Future Oncol* 8(1):55–71.
7. Li AJ, et al. (2004) The prognostic significance of thrombocytosis in epithelial ovarian carcinoma. *Gynecol Oncol* 92(1):211–214.
8. Obermayr E, et al. (2013) Molecular characterization of circulating tumor cells in patients with ovarian cancer improves their prognostic significance: A study of the OVCAD consortium. *Gynecol Oncol* 128(1):15–21.
9. Taylor DD, Gerçel-Taylor C (2005) Tumour-derived exosomes and their role in cancer-associated T-cell signalling defects. *Br J Cancer* 92(2):305–311.
10. Meirelles K, et al. (2012) Human ovarian cancer stem/progenitor cells are stimulated by doxorubicin but inhibited by Mullerian inhibiting substance. *Proc Natl Acad Sci USA* 109(7):2358–2363.
11. Taylor DD, Gercel-Taylor C, Parker LP (2009) Patient-derived tumor-reactive antibodies as diagnostic markers for ovarian cancer. *Gynecol Oncol* 115(1):112–120.
12. Yip P, et al. (2011) Comprehensive serum profiling for the discovery of epithelial ovarian cancer biomarkers. *PLoS ONE* 6(12):e29533.
13. Kinde I, et al. (2013) Evaluation of DNA from the Papanicolaou test to detect ovarian and endometrial cancers. *Sci Transl Med* 5(167):167ra4.
14. Buckanovich RJ, et al. (2007) Tumor vascular proteins as biomarkers in ovarian cancer. *J Clin Oncol* 25(7):852–861.
15. Emmanuel C, et al.; Australian Ovarian Cancer Study Group (2011) Comparison of expression profiles in ovarian epithelium in vivo and ovarian cancer identifies novel candidate genes involved in disease pathogenesis. *PLoS ONE* 6(3):e17617.
16. Oribabor JW, Ambrosio A, Castro CM, Birrer MJ (2012) *Biotargets of Cancer in Current Clinical Practice*, ed Bologna M (Springer/Humana Press, New York), pp 381–402.
17. Kipps E, Tan DS, Kaye SB (2013) Meeting the challenge of ascites in ovarian cancer: New avenues for therapy and research. *Nat Rev Cancer* 13(4):273–282.

18. Attanoos RL, Webb R, Dojcinov SD, Gibbs AR (2002) Value of mesothelial and epithelial antibodies in distinguishing diffuse peritoneal mesothelioma in females from serous papillary carcinoma of the ovary and peritoneum. *Histopathology* 40(3): 237–244.
19. Comin CE, Saieva C, Messerini L (2007) h-caldesmon, calretinin, estrogen receptor, and Ber-EP4: A useful combination of immunohistochemical markers for differentiating epithelioid peritoneal mesothelioma from serous papillary carcinoma of the ovary. *Am J Surg Pathol* 31(8):1139–1148.
20. Laury AR, et al. (2010) PAX8 reliably distinguishes ovarian serous tumors from malignant mesothelioma. *Am J Surg Pathol* 34(5):627–635.
21. Ordóñez NG (1998) Role of immunohistochemistry in distinguishing epithelial peritoneal mesotheliomas from peritoneal and ovarian serous carcinomas. *Am J Surg Pathol* 22(10):1203–1214.
22. Ordóñez NG (2006) The diagnostic utility of immunohistochemistry and electron microscopy in distinguishing between peritoneal mesotheliomas and serous carcinomas: A comparative study. *Mod Pathol* 19(1):34–48.
23. Cancer Genome Atlas Research Network (2011) Integrated genomic analyses of ovarian carcinoma. *Nature* 474(7353):609–615.
24. Elschenbroich S, et al. (2011) In-depth proteomics of ovarian cancer ascites: Combining shotgun proteomics and selected reaction monitoring mass spectrometry. *J Proteome Res* 10(5):2286–2299.
25. Karst AM, Drapkin R (2011) The new face of ovarian cancer modeling: Better prospects for detection and treatment. *F1000 Med Rep* 3:22.
26. Scarberry KE, Dickerson EB, Zhang ZJ, Benigno BB, McDonald JF (2010) Selective removal of ovarian cancer cells from human ascites fluid using magnetic nanoparticles. *Nanomedicine* 6(3):399–408.
27. Uhlen M, et al. (2010) Towards a knowledge-based Human Protein Atlas. *Nat Biotechnol* 28(12):1248–1250.
28. LaRocca PJ, Rheinwald JG (1984) Coexpression of simple epithelial keratins and vimentin by human mesothelium and mesothelioma in vivo and in culture. *Cancer Res* 44(7):2991–2999.
29. Laury AR, et al. (2011) A comprehensive analysis of PAX8 expression in human epithelial tumors. *Am J Surg Pathol* 35(6):816–826.
30. Stussi G, et al. (2005) Isotype-specific detection of ABO blood group antibodies using a novel flow cytometric method. *Br J Haematol* 130(6):954–963.
31. Ng PC, et al. (2004) Neutrophil CD64 is a sensitive diagnostic marker for early-onset neonatal infection. *Pediatr Res* 56(5):796–803.
32. Armstrong DK, White AJ, Weil SC, Phillips M, Coleman RL (2013) Farletuzumab (a monoclonal antibody against folate receptor alpha) in relapsed platinum-sensitive ovarian cancer. *Gynecol Oncol* 129(3):452–458.
33. Teng L, Xie J, Teng L, Lee RJ (2012) Clinical translation of folate receptor-targeted therapeutics. *Expert Opin Drug Deliv* 9(8):901–908.
34. Suh KS, et al. (2010) Ovarian cancer biomarkers for molecular biosensors and translational medicine. *Expert Rev Mol Diagn* 10(8):1069–1083.
35. Latifi A, et al. (2011) Cisplatin treatment of primary and metastatic epithelial ovarian carcinomas generates residual cells with mesenchymal stem cell-like profile. *J Cell Biochem* 112(10):2850–2864.
36. Kalluri R, Weinberg RA (2009) The basics of epithelial-mesenchymal transition. *J Clin Invest* 119(6):1420–1428.
37. Voldman J, Gray ML, Schmidt MA (1999) Microfabrication in biology and medicine. *Annu Rev Biomed Eng* 1:401–425.
38. Xia Y, Whitesides GM (1998) Softlithographie. *Angew Chem Int Ed* 110:568–594.
39. Heitz F, et al. (2012) Bevacizumab in the treatment of ovarian cancer. *Adv Ther* 29(9): 723–735.
40. Carden CP, et al. (2012) The association of PI3 kinase signaling and chemoresistance in advanced ovarian cancer. *Mol Cancer Ther* 11(7):1609–1617.
41. Han L, et al. (2005) The clinical significance of EphA2 and Ephrin A-1 in epithelial ovarian carcinomas. *Gynecol Oncol* 99(2):278–286.
42. Landen CN, Kinch MS, Sood AK (2005) EphA2 as a target for ovarian cancer therapy. *Expert Opin Ther Targets* 9(6):1179–1187.
43. Lee JW, et al. (2009) EphA2 immunoconjugate as molecularly targeted chemotherapy for ovarian carcinoma. *J Natl Cancer Inst* 101(17):1193–1205.
44. Huang CY, et al. (2006) Serum mesothelin in epithelial ovarian carcinoma: A new screening marker and prognostic factor. *Anticancer Res* 26(6C):4721–4728.
45. Bellone S, et al. (2009) Overexpression of epithelial cell adhesion molecule in primary, metastatic, and recurrent/chemotherapy-resistant epithelial ovarian cancer: Implications for epithelial cell adhesion molecule-specific immunotherapy. *Int J Gynecol Cancer* 19(5):860–866.
46. Ghazani AA, Castro CM, Gorbatov R, Lee H, Weissleder R (2012) Sensitive and direct detection of circulating tumor cells by multimarker μ-nuclear magnetic resonance. *Neoplasia* 14(5):388–395.
47. Kristiansen G, et al. (2002) CD24 is expressed in ovarian cancer and is a new independent prognostic marker of patient survival. *Am J Pathol* 161(4):1215–1221.
48. Richter CE, et al. (2010) High-grade, chemotherapy-resistant ovarian carcinomas overexpress epithelial cell adhesion molecule (EpCAM) and are highly sensitive to immunotherapy with MT201, a fully human monoclonal anti-EpCAM antibody. *Am J Obstet Gynecol* 203(6):582.e1–582.e7.
49. Zecchini S, et al. (2011) The adhesion molecule NCAM promotes ovarian cancer progression via FGFR signalling. *EMBO Mol Med* 3(8):480–494.
50. Kachali C, Eltoum I, Horton D, Chhieng DC (2006) Use of mesothelin as a marker for mesothelial cells in cytologic specimens. *Semin Diagn Pathol* 23(1):20–24.
51. Kim JH, et al. (2009) Immunocytochemical panel for distinguishing between adenocarcinomas and reactive mesothelial cells in effusion cell blocks. *Diagn Cytopathol* 37(4):258–261.
52. Choi J-H, Choi K-C, Auersperg N, Leung PCK (2004) Overexpression of follicle-stimulating hormone receptor activates oncogenic pathways in preneoplastic ovarian surface epithelial cells. *J Clin Endocrinol Metab* 89(11):5508–5516.
53. Ji Q, Liu PI, Chen PK, Aoyama C (2004) Follicle stimulating hormone-induced growth promotion and gene expression profiles on ovarian surface epithelial cells. *Int J Cancer* 112(5):803–814.
54. Radu A, et al. (2010) Expression of follicle-stimulating hormone receptor in tumor blood vessels. *N Engl J Med* 363(17):1621–1630.
55. Zheng W, et al. (2000) Ovarian epithelial tumor growth promotion by follicle-stimulating hormone and inhibition of the effect by luteinizing hormone. *Gynecol Oncol* 76(1):80–88.
56. Haber DA, Gray NS, Baselga J (2011) The evolving war on cancer. *Cell* 145(1):19–24.
57. Zorn KK, et al. (2003) Choice of normal ovarian control influences determination of differentially expressed genes in ovarian cancer expression profiling studies. *Clin Cancer Res* 9(13):4811–4818.
58. Chung J, et al. (2013) Rare cell isolation and profiling on a hybrid magnetic/size-sorting chip. *Biomicrofluidics* 7:054107.
59. Chung J, et al. (2012) Microfluidic cell sorter (μFCS) for on-chip capture and analysis of single cells. *Adv Healthc Mater* 1(4):432–436.
60. Daniels VG, Wheater PR, Burkitt HG (1979) *Functional Histology: A Text and Colour Atlas* (Churchill Livingstone, Edinburgh).
61. Malkov VA, et al. (2009) Multiplexed measurements of gene signatures in different analytes using the Nanostring nCounter Assay System. *BMC Res Notes* 2:80.
62. Geiss GK, et al. (2008) Direct multiplexed measurement of gene expression with color-coded probe pairs. *Nat Biotechnol* 26(3):317–325.